Hindawi
Advances in Civil Engineering
Volume 2022, Article ID 6997928, 9 pages
https://doi.org/10.1155/2022/6997928

Research Article

Analysis and Design of the Accessory Structure under the Large Deformation of a Flexible Roof

Shi-chang Zhang,[1,2] **Xiao-ming Xu**,[2] **Feng Gao**,[2] **Peng Huang**,[3] **Bin Luo**,[1] **Wei-zhou Shi**,[2] **and Qing Fang**[2]

[1]*Southeast University, Nanjing 210096, China*
[2]*Arcplus Institute of Shanghai Architectural Design and Research, Shanghai 200041, China*
[3]*Tongji University, Shanghai 200082, China*

Correspondence should be addressed to Shi-chang Zhang; zhangsc@aisa.com.cn

Received 25 November 2021; Revised 8 July 2022; Accepted 24 August 2022; Published 13 September 2022

Academic Editor: Nicola Buratti

Copyright © 2022 Shi-chang Zhang et al. This is an open access article distributed under the Creative Commons Attribution License, which permits unrestricted use, distribution, and reproduction in any medium, provided the original work is properly cited.

An increasing number of large-span space structures use flexible roofs to achieve a light and splendid architectural effect. When a flexible structural system such as a cable net is applied in a large-span stadium, the roof will deform significantly under the self-weight and wind load. Accessory structures of the roof such as catwalks, radial drainage pipes, circular drainage channels, and radial cable trenches need to cooperate with the large deformation of the roof to prevent damage caused by the large deformation of the roof. To thoroughly unveil the analysis and design method of an accessory structure, this paper first carried out the wind tunnel test to determine the wind load of the structure. Then, the gust response factors of each roof area and the dynamic amplification coefficient of the accessory structure considering the roof vibration were determined. Next, circular and radial catwalks were designed based on static analysis. A sliding joint was set in the accessory structure to adapt to the large deformation of the roof. Finally, a time history analysis of the catwalk was carried out to obtain the maximum deformation value of the sliding joint for the safety of the structure. The results demonstrate that the maximum deformation is less than the value given by the design and meets the specification.

1. Introduction

The large-span roof structures are widely used in sports buildings because of their capacity of providing huge space without inner columns [1, 2]. The roof is usually divided into the rigid roof, flexible roof, and rigid-flexible hybrid roof. In recent years, a growing number of stadiums adopt flexible roof structures to achieve soft and polished architectural appearance [3].

The large-span roof structure has the characteristics of lightweight, large flexibility, and small damping. The wind load is generally one of the control loads in the structural design. The damping of the flexible roof is smaller, and the natural frequency is closer to the predominant frequency of the wind, and it is more sensitive to the wind load, especially the fluctuating wind compared with other structures [4]. Consequently, the wind-induced response is ordinarily significant, and the vertical displacement usually far exceeds the limit value of the specification [5]. The roof of sports buildings will be equipped with accessory structures such as radial catwalks, circular catwalks, radial drainage pipes, circular drainage channels, and radial cable trenches. The large deformation of the roof will cause damage to the accessory structure. Therefore, the stress state of the accessory structure under the large deformation of the roof needs to be further analyzed and specially designed.

2. Project Overview

Spoke single-layer cable net as a new flexible structure system was applied to Jaber Ahmed International Stadium [6] for the first time in 2009. This spoke tension structure

evolved from the stress mechanism of the bicycle spoke with the advantages of a simple structural system and clear force transmission path, as shown in Figure 1.

The radial cable is connected to the outer compression ring and the inner tension ring. The cable's tension and the outer ring's pressure are balanced. The overall structure belongs to a self-balancing system. This structure is usually covered with membrane materials, which have lightweight and beautiful appearance characteristics and are mainly applied in large stadiums. The single-layer cable-net structure generally has the ups and downs of the outer compression ring, forming a saddle-shaped spatial curved surface shape. The saddle-shaped roof can provide a sizeable vertical stiffness for the structure.

Suzhou Olympic Sports Center Stadium is the largest spoke single-layer cable-net structure in China [7, 8], as shown in Figure 2. Figure 3 illustrates the main geometric dimensions of the structure. The roof is constructed as a single-layer cable-net structure with a membrane covering and axial diameters of 260 m and 230 m. The height difference of the saddle shape is 25 m, creating the outer contour of the bowl. The maximum height of the structure is 40m, and the radial cable length is between 51 m and 54 m.

The main structure of the stadium is a new supporting system with reasonable stress and high structural efficiency. The structure is made of modern and novel materials to realize a lightweight super large-span space structure. High-strength materials are applied to save natural resources in the structure for environmental protection and the economy. It comprises the outward inclined V-shaped column, saddle-shaped outer compression ring, inner tension ring, and cable net, as shown in Figure 4. The membrane roof is arranged above the cable net structure formed by radial and inner ring cables. The concave radial cable mainly bears the gravity load, and the convex radial cable mainly bears the upward wind suction load, as shown in Figure 5. The radial cable is prestressed and anchored on the outer ring beam. The outer ring beam mainly bears the axial pressure through a reasonable cable net form-finding analysis. It forms a spatial structure with excellent stiffness with a V-shaped column, which can resist horizontal wind loads and earthquakes. All radial cables and circular cables are Galfan-coated full-locked coil ropes [9].

The wind-induced response analysis of the stadium shows that the maximum vertical displacement of the inner ring cable can reach 2.8 m [7], which is far beyond the deformation limit of the code. Therefore, it is necessary to analyze the accessory structure of the roof to avoid damage to the accessory structure caused by the large deformation.

Since there are few such projects in the world and the relevant research is basically blank, Suzhou Olympic Center Stadium was taken as an example to introduce the analysis and design methods to the accessory structure under large deformation of the roof in detail. In Section 3 of this paper, the wind tunnel test was conducted to determine the wind load of the structure, and the dynamic amplification factor of the accessory structure was calculated. In Section 4, the design method of the catwalk was introduced in detail to adapt to the large deformation of the roof. In Section 5, the

Figure 1: The evolution process of spoke single-layer cable net.

Figure 2: The appearance of the stadium.

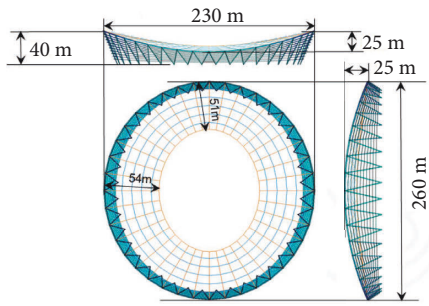

Figure 3: Main dimensions of the roof.

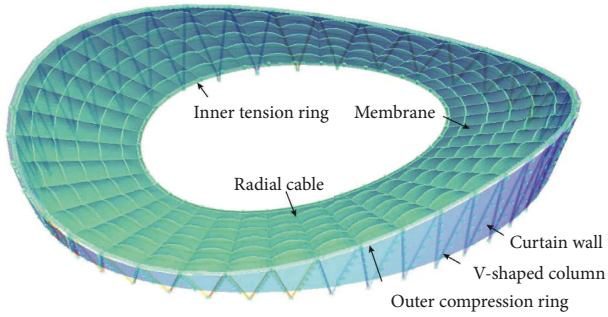

Figure 4: Composition of the main roof structure.

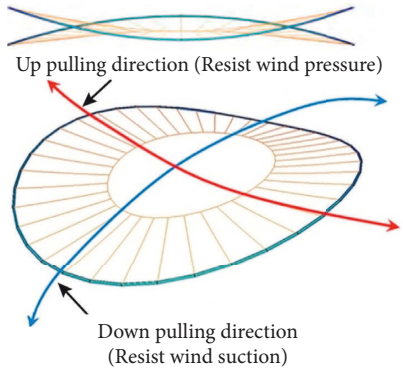

Figure 5: Wind resistance principle.

wind-induced response analysis of the catwalk was carried out, and the results were compared with the results obtained by the design method to ensure the safety of the structure. Finally, Section 6 summarizes the whole study.

3. Wind-Induced Response Analysis

3.1. Wind Tunnel Test. Pressure measurement experiments of rigid models have always been the main wind resistance research method for long-span roof structures [10]. The pressure measurement test of the rigid model ignores the coupling between the structure and the wind [11]. It measures the average and fluctuating wind load acting on the structure. To determine the wind load acting on the structure, a detailed wind pressure measurement was carried out through the rigid model wind tunnel test. The model is made of plexiglass and ABS (acrylonitrile butadiene styrene) plates with sufficient strength and stiffness, as shown in Figure 6. There is no deformation or noticeable vibration under the test wind speed to ensure pressure measurement accuracy.

The geometric scale ratio of the model is 1 : 250, and the shape of the model and the real object is geometrically similar [12]. The wind direction angle in the test was simulated by rotating the turntable. Figure 7 illustrates the definition of the wind direction angle. When the wind blows from the north of the building to the model, it is defined as a 0° wind direction angle. The wind direction angle increases clockwise, and the interval of the wind direction angle is 15° [13]. The structure is divided into four areas A, B, C, and D. The red part is the cantilever end of the roof, and the blue part is the wall and external ring beam. Four hundred forty-three measuring points were arranged on the rigid model. Considering the wind on the inner and outer sides of the wall of the long-span roof structure, a pair of measuring points were arranged at each position, and the pressure of the measuring points is the difference between outer and inner surface pressures [14]. The landform type is class B; the basic wind pressures of the 50-year return period and 100-year return period are 0.45 kPa and 0.50 kPa, respectively, and the corresponding gradient wind speeds are 45.7 m/s and 48.2 m/s. The wind load F_{ji} on the structure is determined by the following formula:

$$F_{ji} = \frac{1}{2}\rho U_i^2 C_{P,ji} A_i, \tag{1}$$

where ρ is the air density, U_i is the wind speed at the height of the ith pressure measuring point, A_i is the auxiliary area of the measuring point, and $C_{P,ji}$ is the wind pressure coefficient at the ith measuring point on the surface of the rigid model. The wind load acting on the actual structure can be obtained by proportional conversion of the wind load in the wind tunnel test.

3.2. Gust Response Factors of the Structure. The wind load time histories obtained from the rigid model wind tunnel test were used to act directly on the corresponding nodes of the roof. The wind-induced vibration response of the structure was analyzed in the time domain through the ANSYS transient analysis method, taking into account the nonlinear geometric effect caused by the large deformation of the structure. The first two vibration modes of the roof are shown in Figure 8. The ring beam and the V-shaped column were simulated by Beam 188, and the cable was simulated by Link 10. The dynamic balance equation of the structure is given by

$$[M]\{\ddot{U}(t)\} + [C]\{\dot{U}(t)\} + [K]\{U(t)\} = \{P(t)\}, \tag{2}$$

where $[M]$, $[C]$, and $[K]$ are the mass matrix, damping matrix, and stiffness matrix of the structure, respectively. $\{U(t)\}$ is the node displacement and $\{P(t)\}$ is the column vector of the structural node load under the action of fluctuating wind. The wind pressure sequence is applied to the finite element model by the Newmark-β method. The wind-induced response of the structure can be obtained by step-by-step integration. The damping of the structure adopts the proportional damping model [15]. Fourteen specific wind directions in the wind tunnel test were selected for calculation.

The wind loads acting on structures under stationary winds have traditionally been treated by the gust response factor method [16, 17] in most major codes and standards worldwide. Based on the theory of stationary random vibration [18, 19], the peak displacement response at a reference height H equals

$$\hat{Y}(H) = \overline{Y}(H) + g\sigma_Y, \tag{3}$$

where $\hat{Y}(H)$ is the mean displacement response, g is the peak factor, taken as 2.5 in the Chinese specification, and σ_Y represents the root mean square (RMS) of the displacement. The gust response factor, which is defined as the ratio of the peak load effect on the structure to the mean load effect corresponding to the design wind speed, can be expressed as follows:

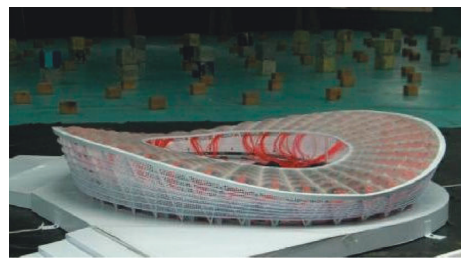

Figure 6: Rigid model of the stadium.

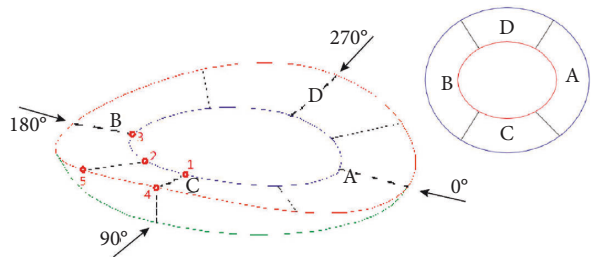

Figure 7: Definition of the wind direction angle.

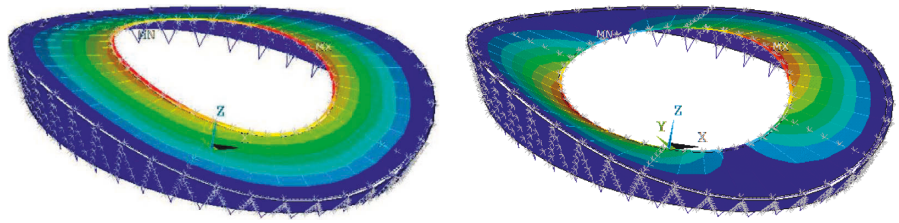

(a) (b)

Figure 8: Main vibration modes of the roof. (a) The first mode (0.429 Hz) and (b) the second mode (0.463 Hz).

$$\beta = \frac{\widehat{Y}(H)}{\overline{Y}(H)} = 1 + \frac{g\sigma_Y}{\overline{Y}(H)}. \quad (4)$$

Figure 9 presents the time histories of the vertical displacement of the cantilever end in areas A, B, C, and D under the control wind direction. The gust response factor β of each area can be calculated by Formula (4), which is listed in Table 1. From the vertical displacement time histories of the roof cantilever end in each area, it can be observed that the vertical displacement of the cantilever end in area C is the largest, which is the most unfavorable working condition. Therefore, the gust loading factor of the whole roof can be subject to the result of area C, taken as 1.90. Through the gust loading factor, the equivalent static wind load of the structure can be determined to carry out the subsequent static analysis.

3.3. Dynamic Amplification Factor of the Accessory Structure. The roof vibrates under the wind load, and the dynamic amplification caused by the roof vibration should be considered for the accessory structure. The accessory structure's dynamic amplification factor (DAF) was calculated by analyzing the vertical acceleration of the cantilever end. Figure 10 shows the cantilever's vertical acceleration time histories in area D and the acceleration power spectral density (PSD). The maximum variance of the acceleration root reaches 2.575 m/s^2. The dynamic amplification factor can be obtained by Formula (4):

$$\mathrm{DAF} = \frac{g_1 + g\sigma_a}{g_1}, \quad (5)$$

where $g_1$is gravity acceleration, taking a value of 9.8 m/s^2, and σ_a is the RMS of acceleration. Therefore, the dynamic amplification factor of area D can be given by DCF = (9.8 + 2.5×2.575)/9.8 = 1.66. The dynamic amplification factor and the control wind direction angle of each area are shown in Table 2. Considering this dynamic amplification factor, the static analysis of the accessory structure is carried out to consider the dynamic influence of roof vibration under wind-induced action.

4. Static Analysis of the Accessory Structure

4.1. Deformation Analysis of the Catwalk. The design idea of an accessory structure is actively adapted to the roof's large deformation, so many sliding connection nodes and rotating connection nodes are set in the accessory structure. This can reduce the adverse effects of the large roof deformation and the stiffness of the accessory structures [20], avoiding unnecessary secondary stress and making the main structure analysis closer to reality. Unstructured connecting elements are set in the overall model to simulate and analyze the deformation of the accessory structure, as shown in Figure 11. The element is equivalent to a linear spring, so the deformation of the connecting element is the release demand of the sliding node of the accessory structure. The total length of the circular catwalk is 435 m, which is simulated by 40 unstructured connection elements (Nos. 0–39).

Figure 12 illustrates each element's deformation under different working conditions. It can be seen that the expansion amount of each element is −5.0 mm to 11.3 mm (tension is defined by a positive sign and pressure is defined by a negative sign). The radial catwalk is simulated by six unstructured elements (Nos. 1 to 6), and four radial catwalks (axes 1 to 4) are selected for analysis. Figure 13 displays the envelope values of tension (max) and compression (min) of the four radial catwalks under different working conditions. It can be seen that the deformation of each component of the radial catwalk is large.

4.2. Design of the Circular Catwalk. For the purpose of meeting the architectural requirements for the roof, the traditional "hanging" form was abandoned for the catwalk. All catwalks are turned up and arranged above the cable head at the intersection of the inner ring cable and the radial cable to ensure that spectators cannot see catwalk components. The circular catwalk is divided into two cases, catwalk with lamps and catwalk without lamps, considering lighting layout requirements. The three-dimensional diagram of the circular upturned catwalk is shown in Figure 14.

Two transverse beams connect the supporting columns on the adjacent ring cable clamps on the circular catwalk. The maximum span of the beam is nearly 12 m. Two railing columns are set at the three equally divided positions on the cross beam of each span to reduce the span of the upper transverse member, as shown in Figure 15. The main stress-bearing component of the circular catwalk is transverse beams, and both sides are hinged with the ring cable clamp through the support column. Under structural deformation, the transverse beam is always parallel to each ring cable. Therefore, the deformation to be set for the beam sliding joint is the envelope value of the ring cable's deformation under various working conditions. Based on the deformation of the circular connecting element, a deformation of

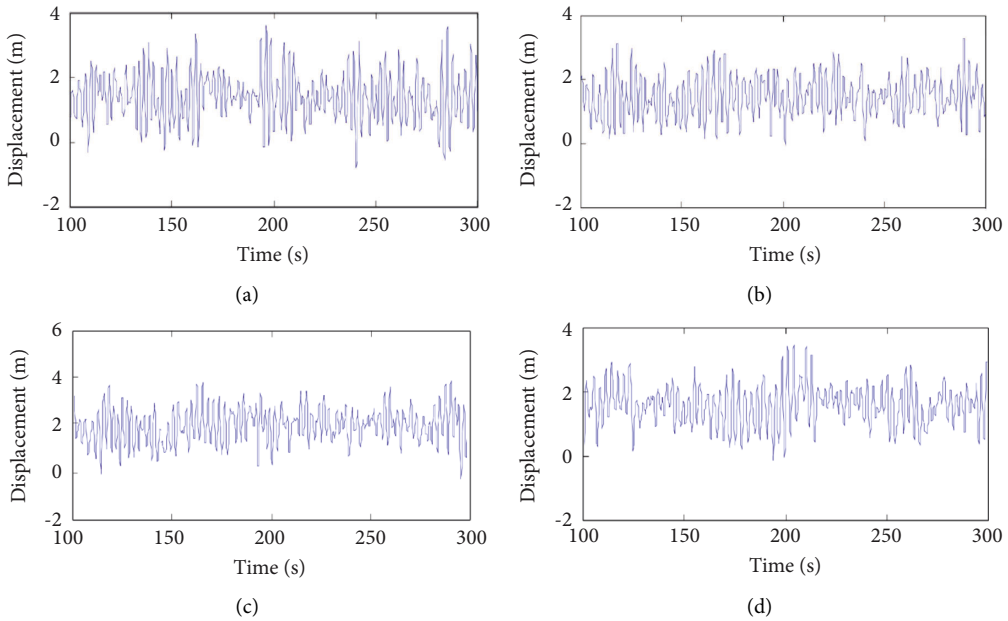

Figure 9: Vertical displacement time histories of the cantilever end in different areas. (a) Area A (75° wind angle). (b) Area B (90° wind angle). (c) Area C (90° wind angle). (d) Area D (240° wind angle).

Table 1: Gust response factor of each area.

Response type Vertical displacement of the roof cantilever end	Area A	Area B	Area C	Area D
Control wind direction	75°	90°	90°	240°
Gust loading factors	2.33	2.14	1.86	2.01

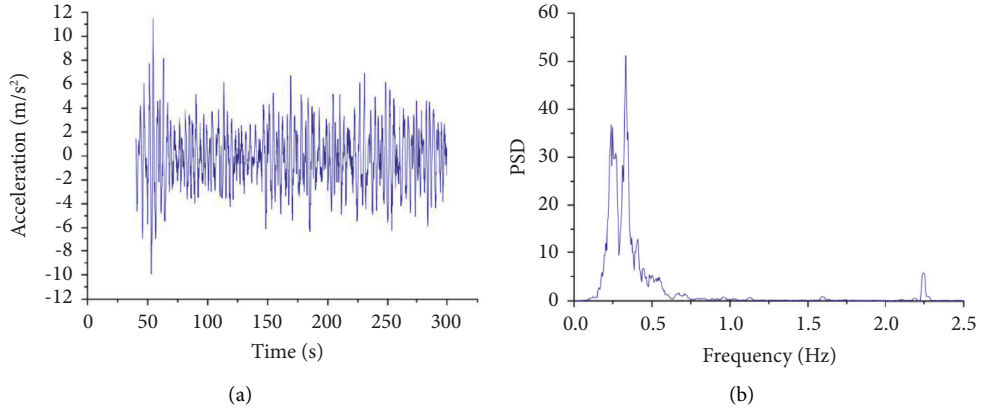

Figure 10: Vertical acceleration at the cantilever end in area D. (a) Acceleration time history and (b) PSD of acceleration.

Table 2: Dynamic amplification factor and the control wind direction angle.

Response type Vertical displacement of the roof cantilever end	Area A	Area B	Area C	Area D
Control wind direction	105	60	105	90
Acceleration root variance (m/s^2)	2.226	2.209	1.644	2.575
DAF	1.57	1.56	1.42	1.66

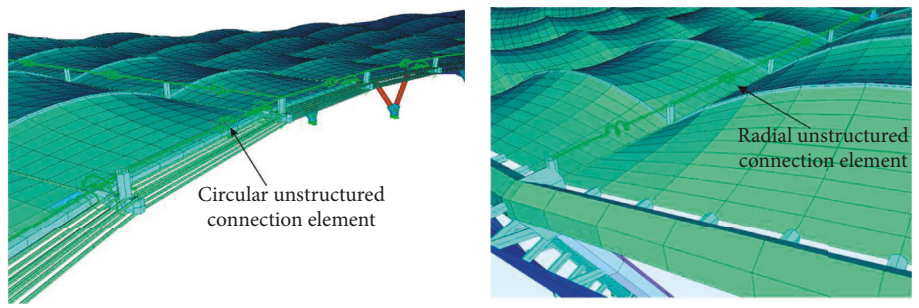

Figure 11: Calculation model of the accessory structure. (a) Circular catwalk. (b) Radial catwalk.

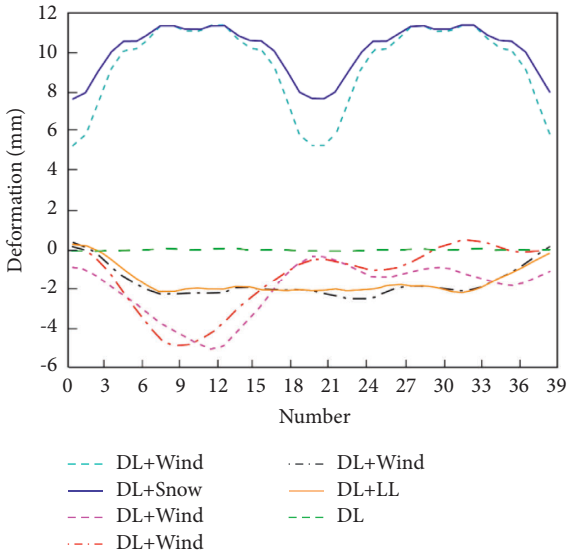

Figure 12: Circular connection element.

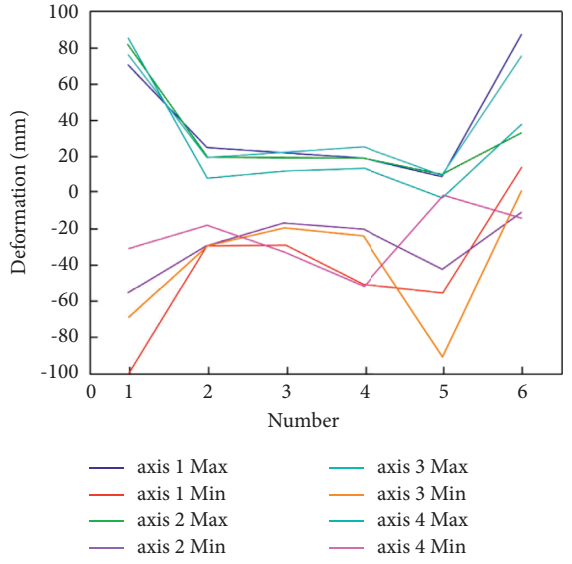

Figure 13: Radial connection element.

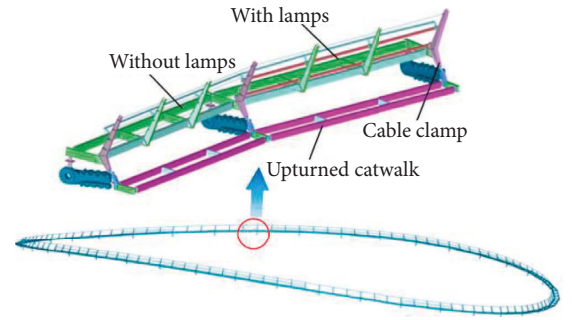

Figure 14: 3D diagram of the circular catwalk.

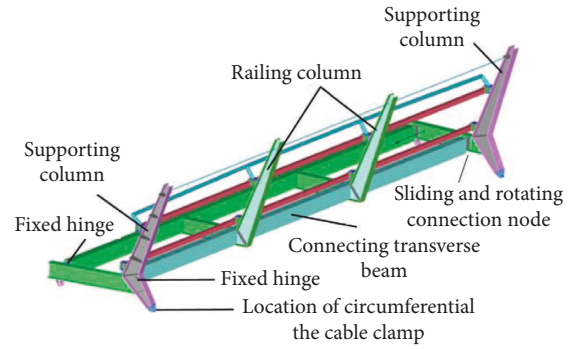

Figure 15: Structure composition of the circular catwalk.

20 mm is reserved for the sliding joint. One end adopts a fixed hinge, and the other adopts a hinge plus axial sliding. The detailed structure is shown in Figure 16.

4.2.1. Catwalk without Lamps. The railing column is set on the transverse beam. The railing column is rigidly connected to the beam. When there is a significant vertical deformation difference between adjacent cable clamps, the railing will turn a certain angle with the deformation of the beam, resulting in a large amount of deformation of the side span. If the conventional three-span railing is adopted, the nodes of the side spans on both sides need to reserve a large amount of deformation, increasing the node length. Meanwhile, the large number of nodes will increase the load of the inner ring cable, resulting in difficulties in processing and a poor overall effect on the building. After studying the

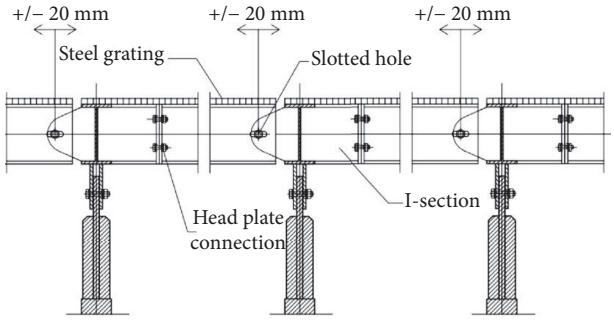

Figure 16: The detailed structure of the circular catwalk.

deformation mechanism of the single-span catwalk, it can be found that when the vertical relative deformation δ occurs on the catwalk, the total length of the three sections of railings between adjacent cable clamps remains unchanged, as shown in Figure 17. Therefore, we abandoned the traditional railing and changed it to a single-span cable, as shown in Figure 18. The cable is only anchored to the supporting column on the cable clamp, a circular hole is set on the railing column, and the cable passes through the circular hole. The inner wall of the hole is provided with an EPDM (ethylene propylene diene monomer) protective sleeve to avoid scratching the cable, as shown in Figure 19. The cable makes the overall appearance effect of the catwalk concise and eliminates the cumbersome railing release node. The cable material is stainless steel, which has the advantages of a low elastic modulus and a strong ability to adapt to deformation.

4.2.2. Catwalk with Lamps. When lamps are installed on the catwalk, the load of the lamps is significant, and a reciprocating dynamic load will be generated under the wind-induced vibration response. In this case, if a 12 m beam is used to support the lamp, the span is too large, resulting in a large deflection, which is unfavorable to the structure. Therefore, the lamp beam was segmented to reduce its calculated length, and support nodes were set up, as shown in Figure 20. The lamp beam has significant torque because the lamp load is large and has an inclination angle. The support node adopts the form of a double ear plate so that the lamp beam can rotate and expand axially along the pin shaft and effectively transmit the lamp's torque.

Due to the rigid connection between the railing column and the transverse beam, when the beam is deformed, the length of the middle span lamp beam remains unchanged, which only causes the sliding of the side span lamp beam. Therefore, fixed hinge joints are adopted on both sides of the middle span lamp beam, and the side span lamp beam adopts joints with one end hinged and one end sliding axially. The maximum deformation of the lamp beam can reach 50 mm to ensure its safety. To reduce the node size, each side of the node releases ±25 mm deformation.

4.3. Design of the Radial Catwalk. The radial catwalk is canceled due to the large deformation of the radial cable. The upper part of the radial cable is covered with a protective

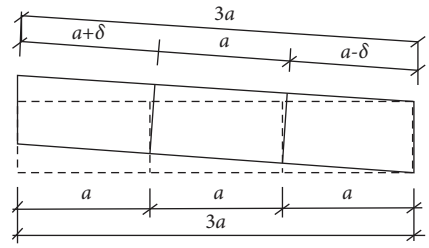

Figure 17: Deformation mechanism of the catwalk.

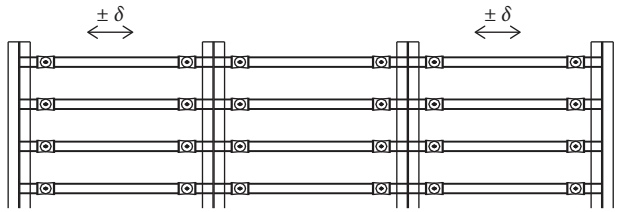

Figure 18: Traditional railing.

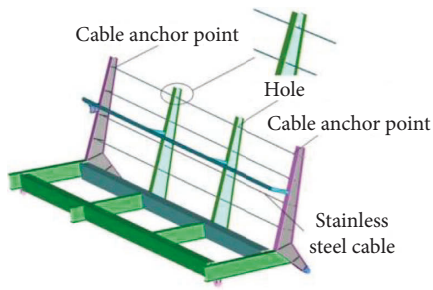

Figure 19: Improved railing.

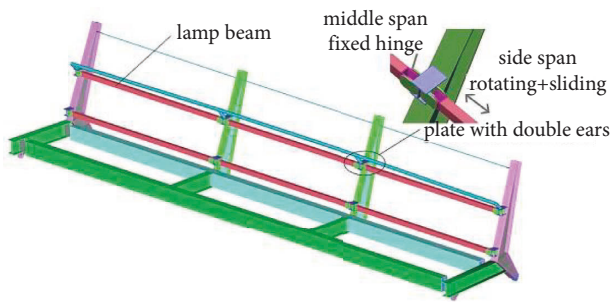

Figure 20: Catwalk with lamps.

film, which forms a natural berm by using the load-bearing characteristics of the membrane structure. Staff can reach the inner circular berm when walking on the protective film. The cable is placed on the radial berm. It can be seen from Figure 21 that the deformation of each component needs to be effectively released. Therefore, slotted holes of +90/−90 mm are adopted for each section of cable route components. Figure 21 shows the detailed structure of the radial components. Through the catwalk set by the protective film and the slotted holes set between the components, the radial secondary components have enough flexibility to adapt to the large deformation of the structure.

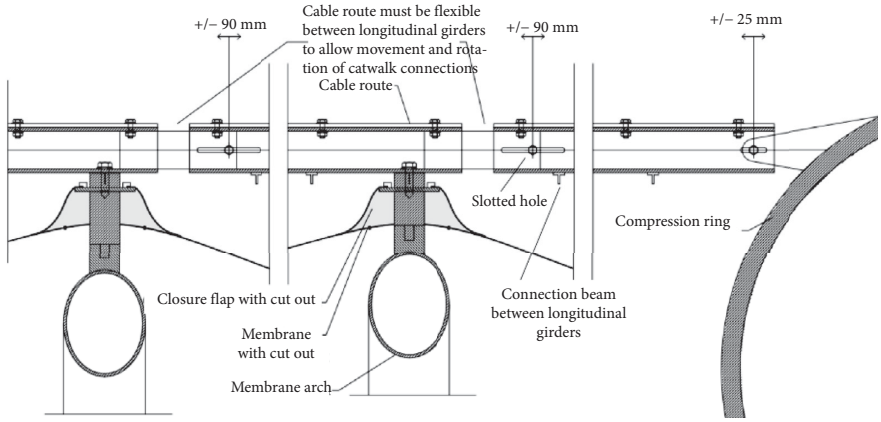

Figure 21: Details of the radial members.

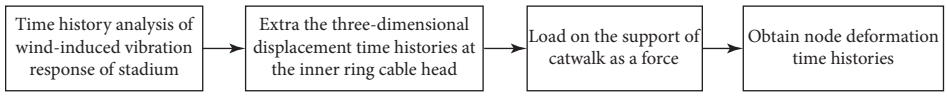

Figure 22: Analysis method of the wind-induced response of the circular catwalk.

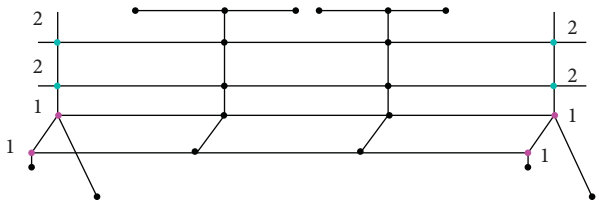

Figure 23: Local analysis model of the circular catwalk.

5. Wind-Induced Response Analysis of the Circular Catwalk

To avoid incomplete consideration of the static analysis, the wind-induced response dynamic analysis of the catwalk was carried out, and the analysis method is shown in Figure 22. First, the gymnasium's wind-induced response time history analysis was carried out. Then, the three-dimensional displacement time history of the inner ring cable head is extracted and applied to the support of the catwalk as an input load to obtain the time history curve of node deformation. The maximum deformation of the joint is compared with the static analysis results.

The local finite element model of the circular berm is shown in Figure 23. The nodes are divided into two types: the first type is the transverse beam node and the second type is the lamp beam node. The top ten maximum deformations of the beam node at the bottom of the circular catwalk are shown in Table 3, and the maximum deformation reaches 10 mm. The top ten maximum deformations of the lamp beam nodes are shown in Table 4, up to 33 mm. The demand value of node expansion is less than the reserved number of nodes in the design (transverse beam: 20 mm and lamp beam: 50 mm).

Table 3: The maximum expansion of the type 1 node.

Wind direction angle (°)	Average value (mm)	Pulsation value (mm)	Maximum (mm)
90	5.0	2.0	10.0
90	5.0	2.0	10.0
90	5.9	1.8	10.0
90	3.9	2.3	10.0
90	−3.8	2.3	10.0
90	4.8	1.7	10.0
90	3.5	2.3	9.0
90	3.2	2.2	8.0
45	−2.0	2.0	7.0
225	2.5	1.8	7.0

Table 4: The maximum expansion of the type 2 node.

Wind direction angle (°)	Average value (mm)	Pulsation value (mm)	Maximum (mm)
90	13.0	8.1	33.0
90	−12.0	7.2	30.0
90	−11.8	7.3	30.0
90	−14.5	6.2	30.0
90	10.0	6.1	25.0
90	10.0	5.0	22.0
270	−12.1	4.2	22.0
270	8.5	4.6	20.0
270	7.8	4.9	20.0
270	6.9	4.4	18.0

6. Conclusion

In this paper, the analysis process and design countermeasures of the accessory structure under the large deformation of the inner ring are given in detail based on the engineering background of Suzhou Olympic Sports Center Stadium. The relevant conclusions are as follows:

(1) Through the wind tunnel test of the rigid model of the stadium, the wind load time history is obtained, and the time history analysis of the stadium is carried out. The vertical displacement of the cantilever end in area C is the largest, and the gust response factor of the whole roof can be subject to area C, which is taken as 1.90.

(2) The roof vibrates under the wind load, and the dynamic amplification caused by the roof vibration should be considered for the accessory structure. The dynamic amplification factor is obtained from the acceleration response, which is 1.66.

(3) The accessory structure needs to set sliding joints to adapt to the large deformation of the roof. The innovation of the accessory structure in this paper lies in that a double ear plate with a slotted hole is set on the lamp beam, which can effectively transmit torque while adapting to telescopic deformation. The cable is used to replace the traditional railing to avoid complex joints.

(4) The deformation of the sliding joint is determined by static analysis. The time history analysis of the accessory structure shows that the maximum deformation of the sliding joint does not exceed the design value.

Data Availability

The data used in this paper are derived from independent analysis of participants during the study.

Conflicts of Interest

The authors declare that they have no conflicts of interest.

Acknowledgments

This work was supported by the National Natural Science Foundation of China under project number 11673039.

References

[1] S. M. Maxwell, F. Kershaw, C. C. Locke et al., "Potential impacts of floating wind turbine technology for marine species and habitats," *Journal of Environmental Management*, vol. 307, Article ID 114577, 2022.

[2] M. Bagheri, A. Chahkandi, and H. Jahangir, "Seismic reliability analysis of RC frames rehabilitated by glass fiber-reinforced polymers," *International Journal of Civil Engineering*, vol. 17, no. 11, pp. 1785–1797, 2019.

[3] L. Shi, W. Yang, K. Chen et al., "Performance Evaluation of W Shape Dynamic Inter-array cable Configuration for Floating Offshore Wind Turbine," in *Proceedings of the Offshore Technology Conference*, Houston, TX, USA, May 2022.

[4] X. Fu, W. L. Du, H. N. Li, and G. Li, "A closed-form solution for the wind-induced responses of transmission lines considering the failure of adjacent towers," *Journal of Wind Engineering and Industrial Aerodynamics*, vol. 228, no. 228, Article ID 105110, 2022.

[5] China Architecture & Building Press, *GB 50009-2012 Loading Code for the Design of Building Structure*, China Architecture & Building Press, Beijing, China, 2012.

[6] B. Annette and S. P. Cacho, *Light Structures*, China Architecture & Building Press, Beijing, China, 2004.

[7] X. M. Xu, S. C. Zhang, and F. Gao, "Structural design on steel roof of stadium of Suzhou olympics sports center," *Building Structure*, vol. 49, no. 23, pp. 1–6, 2019.

[8] S. C. Zhang, X. M. Xu, and W. Z. Shi, "Structural design on stands of stadium of Suzhou olympics sports center," *Building Structure*, vol. 49, no. 23, pp. 8–11, 2019.

[9] S. C. Zhang, X. M. Xu, F. Gao, B. Luo, W. Z. Shi, and Q. Fang, "Experimental study on corrosion of galfan-coated full-locked coil ropes in a natatorium environment," *Advances in Civil Engineering*, vol. 2022, Article ID 9777836, 14 pages, 2022.

[10] X. F. Yu, Z. N. Xie, and M. Gu, "Coupling vibration between wind-induced internal pressure and a flexible roof for buildings with a dominant opening and background leakage," *KSCE Journal of Civil Engineering*, vol. 23, no. 9, pp. 4075–4084, 2019.

[11] X. Zhou and M. Gu, "Test study of wind pressure coefficient on long-span roof," *Journal of Tongji University*, vol. 30, no. 12, pp. 1423–1428, 2002.

[12] H. J. Gerhardt and C. Kramer, "Effect of building geometry on roof windloading," *Journal of Wind Engineering and Industrial Aerodynamics*, vol. 43, no. 1-3, pp. 1765–1773, 1992.

[13] X. Fu, Y. Jiang, W. L. Du, and B. W Yan, "A new radial spoiler for suppressing vortex-induced vibration of a tubular tower and its practical design method," *Shock and Vibration*, vol. 2021, no. 12, 10 pages, Article ID 6971178, 2021.

[14] H. Yasui, H. Marukawa, J. Katagiri, A. Katsumura, Y. Tamura, and K Watanabe, "Study of wind-induced response of long-span structure," *Journal of Wind Engineering and Industrial Aerodynamics*, vol. 83, no. 1-3, pp. 277–288, 1999.

[15] Y. He, S. Dong, and J. Gong, "Wind-induced response of spatial structures with mode compensation in frequency domain," *Engineering Mechanics*, vol. 19, no. 4, pp. 1–6, 2002.

[16] A. G. Davenport, "Gust loading factors," *Journal of the Structural Division*, vol. 93, no. 3, pp. 11–34, 1967.

[17] Y. Zhou and A. Kareem, "Gust loading factor: new model," *Journal of Structural Engineering*, vol. 127, no. 2, pp. 168–175, 2001.

[18] J. D. Holmes, "Distribution of peak wind loads on a low-rise building," *Journal of Wind Engineering and Industrial Aerodynamics*, vol. 29, no. 1-3, pp. 59–67, 1988.

[19] J. D. Holmes, "Effective static load distributions in wind engineering," *Journal of Wind Engineering and Industrial Aerodynamics*, vol. 90, no. 2, pp. 91–109, 2002.

[20] Y. M. Li and X. M. Xu, "Structural design of shanghai oriental sports center comprehensive pavilion," *Building Structure*, vol. 41, no. 12, pp. 711–715, 2011.